First-principles study of lattice dynamics and thermodynamic properties of LaCl₃ and LaBr₃

Bo Liu,[1,*] Mu Gu,[1] Zeming Qi,[2] Xiaolin Liu,[1] Shiming Huang,[1] and Chen Ni[1]

[1]*Laboratory of Waves & Microstructure Materials, Pohl Institute of Solid State Physics, Tongji University, Shanghai 200092, China*
[2]*NSRL, University of Science and Technology of China, Hefei 230027, China*

We perform first-principles calculations of the lattice dynamics and the thermodynamic properties of LaCl₃ and LaBr₃. Using density-functional perturbation theory, we obtain the Born effective charge tensors, the dielectric permittivity tensors, the phonon frequencies at the Brillouin zone center, and the phonon dispersion curves, as well as corresponding density of states. The Born effective charge and the dielectric permittivity tensors exhibit anisotropy, which are analyzed in detail. The calculated phonon frequencies at the Γ point of the Brillouin zone show good agreement with the experimental values for most vibrational modes. The light yields of LaCl₃ : Ce and LaBr₃ : Ce are theoretically estimated to be 62 400 and 71 400 photons/MeV, respectively, on the basis of the calculated values of the dielectric constants and the highest longitudinal optical infrared phonon frequencies. The thermodynamics properties including the phonon contribution to the Helmholtz free energy ΔF, the phonon contribution to the internal energy ΔE, the entropy S, and the constant-volume specific heat C_v are determined within the harmonic approximation based on the calculated phonon dispersion relations.

PACS number(s): 63.20.Dj, 65.40.Ba, 77.22.Ch

I. INTRODUCTION

Nowadays, lanthanide trihalides hosts are the very important host materials for the development of new inorganic scintillators. The cerium-doped lanthanide trihalides LaCl₃ : Ce and LaBr₃ : Ce have been extensively studied as scintillators with the remarkably high light yields of 46 000 and 63 000 photons/MeV, respectively.[1–7] At present, LaBr₃ : Ce is the brightest commercially available scintillators. They have very good energy resolution and their decay times are shorter than 30 ns without intense slow component under γ-ray excitation,[3,5] which supports counting applications at very high rate.

Lattice vibration can severely affect the luminescent quantum efficiency through the nonradiative transitions of multiphonon orbit-lattice relaxation of excited states of doped rare-earth ions in crystals.[8,9] Although the present work does not deal with the multiphonon transition, determination of the phonon frequencies in LaCl₃ and LaBr₃ is an important basis for the further understanding of the multiphonon transition process, and thus the luminescence efficiencies.

The phonons at Γ point of the Brillouin zone are involved in the optical behavior in crystal. The Raman spectra of LaCl₃ (Ref. 10) and LaBr₃ (Ref. 11) was used to investigate the Raman-active lattice vibrational modes. Symmetry coordinates analysis was made and the infrared-active phonons were demonstrated by infrared absorption spectrum of LaCl₃.[12] The lattice vibrational spectra of LaCl₃ and LaBr₃ were investigated to experimentally determine the phonon frequencies through doping rare-earth ion such as Pr^{3+} as probe, assuming that the vibrational spectra were essentially unchanged with the doped rare-earth ion.[13,14] However, since the inelastic neutron-scattering measurement cannot be found in the literature, the experimental data of phonon frequencies are limited to the Γ point. The dielectric tensors of LaCl₃ and LaBr₃ were obtained by the measurement of electric field polarized reflectance spectra, showing the strong

anisotropic properties due to the hexagonal crystal structure.[15] Therefore the first-principles calculations are highly desirable in order to obtain a deep understanding of fundamental properties of LaCl₃ and LaBr₃.

In this work, we use density-functional perturbation theory to study the dynamical and the dielectric properties of LaCl₃ and LaBr₃. We compute the Born effective charge tensors, the dielectric permittivity tensors, the phonon frequencies at the Brillouin zone center, the phonon dispersion curves, and the thermodynamics properties.

The present paper is organized as follows. In Sec. II, the details of the calculation are described. In Sec. III, the calculated results are presented and discussed in comparison with the available experimental data. In Sec. III A, the study of the structural properties of LaCl₃ and LaBr₃ are reported. In Sec. III B, the Born effective charge tensors are given and analyzed in detail. The lattice vibrational properties, including the phonon frequencies at the Γ point of the Brillouin zone and the phonon dispersion relations along the high symmetry lines of the Brillouin zone as well as the corresponding density of states, are given and discussed with the available experimental results in Sec. III C. The calculated dielectric permittivity tensors are reported and compared with the experiments in Sec. III D. Section III E is devoted to the thermodynamic properties, including the phonon contribution to the Helmholtz free energy, the phonon contribution to the internal energy, the entropy, and the constant-volume specific heat. Finally, the main results and conclusions are summarized in Sec. IV.

II. CALCULATIONAL METHODS

All calculations are performed using the ABINIT package[16,17] which is based on pseudopotentials and plane waves. It relies on an efficient fast Fourier transform algorithm[18] for the conversion of wave functions between real and reciprocal space, on the adaptation to a fixed potential of the band-by-band conjugate gradient method[19] and on

a potential-based conjugate-gradient algorithm[20] for the determination of the self-consistent potential. Exchange and correlation are treated in the local density approximation (LDA) to DFT, using Perdew-Wang's parametrization[21] of Ceperley-Alder electron-gas data.[22] The Hartwigsen, Goedecker, and Hutter (HGH) pseudopotential[23] is used for La $(5s, 5p, 5d, 6s)$ levels treated as valence states. Troullier-Martins[24] pseudopotentials, generated thanks to the FHI98PP code,[25] are used for Cl $(3s, 3p)$ and Br $(4s, 4p)$ levels treated as valence states. Relaxation of the lattice parameters and interatomic positions within the unit cell is performed using the Broyden-Fletcher-Goldfarb-Shanno algorithm[26,27] until the maximum component of force acting on any atoms is less than 1 mH/Bohr.

Linear response properties such as the Born effective charge tensors and the phonon frequencies are obtained as second-order derivatives of the total energy with respect to an external electric field or to atomic displacements within the framework of density functional perturbation theory.[28–30] The linear response method allows the calculation of the dynamical matrix at arbitrary q vectors. The force constants are extracted from a Fourier transform of the dynamical matrices obtained for a grid in the Brillouin zone (BZ). There are later employed to obtain the phonon frequencies at arbitrary points in reciprocal space and the phonon-dispersion relations by interpolation. The phonon density of states is also calculated using these force constants. The wave functions are expanded in plane waves up to a kinetic energy cutoff of 70 Ha. The BZ is sampled by a $4 \times 4 \times 4$ Monkhorst-Pack[31] mesh of k points. Convergence tests show that the BZ sampling and the kinetic energy cutoff are sufficient to guarantee an excellent convergence within 1 cm^{-1} for the calculated phonon frequencies. The phonon band structures based on interatomic force constants are obtained by Fourier interpolation with specific treatment of the long-range dipole-dipole interaction.[28] The role of spin-orbit coupling is considered for the calculation of phonon frequencies at the Γ point.

III. RESULTS AND DISCUSSIONS

A. Structural properties

LaCl$_3$ and LaBr$_3$ are isostructural and have very similar static crystalline electric fields[32] with C_{3h} symmetry at the site of the rare-earth ion. They have a hexagonal dipyramidal type of symmetry and belong to the space group $P6_3/m$ (C_{6h}^2).[33] The primitive cell consists of two molecules, shown in Fig. 1. The La atoms are located in the $2c$ Wyckoff sites $(1/3, 2/3, 1/4)$ and $(2/3, 1/3, 3/4)$. The $X = (Cl, Br)$ atoms occupy the $6h$ Wyckoff sites $(u, v, 1/4)$, $(1-v, u-v, 1/4)$, $(1-u+v, 1-u, 1/4)$, $(u-v, u, 3/4)$, $(1-u, 1-v, 3/4)$ and $(v, 1-u+v, 3/4)$, where u and v are internal parameters. Table I summarizes our results obtained after relaxation of the lattice constants, as well as the experimental values. The calculated lattice constants are underestimated with the maximal error of 2.2%, which is typically the expected precision for the LDA. This reflects the reliability of our self-consistent calculations and the pseudopotentials.

B. Born effective charge tensors

For insulators, the Born effective charge tensor $Z^*_{\kappa, \beta\alpha}$ is defined as the proportionality coefficient relating, at linear
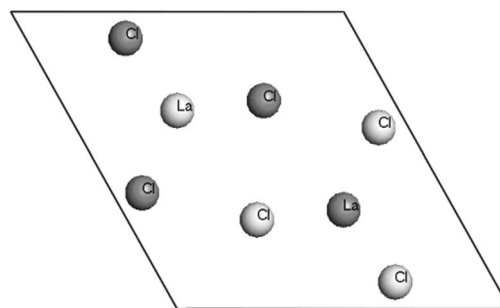

FIG. 1. Structure of LaCl$_3$. The ions in the $\frac{1}{4}c$ plane are dark color balls and the ions in the $\frac{3}{4}c$ plane are light color balls. LaBr$_3$ has the same structure but different lattice constants.

order, the polarization per unit cell, created along the direction β, and the displacement along the direction α of the atoms belonging to the sublattice κ, under the condition of a zero electric field:[30]

$$Z^*_{\kappa, \beta\alpha} = \Omega_0 \frac{\partial P_\beta}{\partial \tau_{\kappa\alpha}}, \qquad (1)$$

where Ω_0 is the unit cell volume.

The Born effective charge tensors of La and $X = (Cl, Br)$ atoms are reported in Table II. The form of effective charge tensor for the constituents is dependent on the site symmetry of the ions. The point symmetry at the site of a La ion is C_{3h} ($2c$ sites) while the point symmetry at a halogen ion site is C_s ($6h$ sites). The matrices for equivalent sites are obtained by the point group rotations. As a consequence, the values of Z_{La}^* are almost diagonal with an anisotropy of 19.3 and 18.7 % for LaCl$_3$ and LaBr$_3$, respectively. They have only two independent components: parallel and perpendicular to the c axis. For the halogen ions $X = (Cl, Br)$, Z_X^* are also shown to be almost diagonal, but with three independent components, shown to be quite anisotropic. The values of Z_{La}^* are anomalously large compared with the nominal ionic charge $Z = +3$, indicating a mixed covalent-ionic bonding.[34] This behavior has also been observed in the case of La$_2$O$_3$ and La$_2$O$_2$S [35,36]. This tendency can be explained from the view point that the Born effective charge depends on the electronic charge reorganization induced by atomic displacements. Since the Born effective charge is dynamical charge, contrary to the static charge, consequences of the covalence effects are to increase the amplitude of Z^*. As can be seen in

TABLE I. Calculated lattice parameters of LaCl$_3$ and LaBr$_3$ compared to experimental values. The length unit is Å.

	LaCl$_3$		LaBr$_3$	
	Theor.	Expt.	Theor.	Expt.
a	7.312	7.468	7.777	7.951
c	4.282	4.366	4.413	4.501
u	0.385	0.375	0.382	0.390
v	0.308	0.292	0.297	0.300
Volume	198.40	211.01	231.12	246.40

TABLE II. Calculated Born effective charge tensors for La and $X=(\text{Cl}, \text{Br})$ atoms in LaCl$_3$ and LaBr$_3$. The nominal charges of La, Cl, and Br are, respectively, $+3$, -1, and -1.

	LaCl$_3$			LaBr$_3$		
La	3.71	−0.03	0	3.69	−0.05	0
	0.03	3.71	0	0.05	3.69	0
	0	0	4.60	0	0	4.54
X	−0.63	0.01	0	−0.66	0.03	0
	−0.01	−1.85	0	−0.03	−1.80	0
	0	0	−1.53	0	0	−1.51

Table II, the values of $Z_{\text{La}}{}^*$ for LaCl$_3$ are slightly larger by 1.3 and 0.5 % in parallel and perpendicular to the c axis, respectively, than those of LaBr$_3$. Such difference can be contributed from the stronger covalent characteristic for the La-Cl bond.

C. Vibrational properties

We calculate the phonon frequencies at the Γ point for LaCl$_3$ and LaBr$_3$. Since there are eight atoms in the primitive cell, there are a total of 24 modes of vibration. The theoretical group analysis predicts the following irreducible representations of acoustical and optical zone-center ($q=0$) modes

$$\Gamma_{\text{aco}} = A_u \oplus E_{1u}$$

for acoustic modes and

$$\Gamma_{\text{opt}} = 2A_g \oplus A_u \oplus 2B_g \oplus 2B_u \oplus E_{1g} \oplus 3E_{2g} \oplus 2E_{1u} \oplus E_{2u}$$

for optical modes.

The A_g, E_{1g}, and E_{2g} modes are Raman active, the A_u and E_{1u} modes are infrared active, and the B_g, B_u, and E_{2u} modes are neither Raman nor infrared active (silent modes). The crystal symmetry contains the inversion operation, so that the Raman and infrared vibrations are mutually exclusive. Before the acoustic sum rule (ASR) is applied, the errors in the acoustic frequencies are 0.424, 0.430, 0.656 cm^{-1} for LaCl$_3$ and 0.282, 0.288, 0.561 cm^{-1} for LaBr$_3$. In Table III, the calculated phonon frequencies for LaCl$_3$ and LaBr$_3$ are presented as well as the experimental values in the literature. When the spin-orbit coupling effect is considered, the maximal differences of phonon frequencies at Γ point are 0.12 and 0.06 cm^{-1} for LaCl$_3$ and LaBr$_3$, respectively. Since the differences are very small, the spin-orbit coupling is neglected for the phonon dispersion calculations. The present calculations predict six Raman-active modes. The Raman spectrum of LaCl$_3$ measured by Asawa *et al.* showed five Raman lines (two A_g, one E_{1g}, and two E_{2g}) but one E_{2g} was missing.[10] The comparison between the calculational and the Raman frequencies gives the maximum deviation of 17 cm^{-1}, a rms of absolute deviations of 9.5 cm^{-1}, and a rms of relative deviations of 6.4%. The phonon frequencies from

TABLE III. Calculated phonon frequencies (cm^{-1}) at the Γ point of the Brillouin zone and the mode assignments for LaCl$_3$ and LaBr$_3$. Experimental values are also shown for comparison.

| Mode | LaCl$_3$ | | | | | LaBr$_3$ | | |
	Present Cal.	Ref. 10 Expt.	Ref. 14 Expt.	Ref. 12 Expt.	Ref. 12 Cal.	Present Cal.	Ref. 11 Expt.	Ref. 14 Expt.
Raman								
$A_g(1)$	185.2	180		177.3	176	111.8	116	
$A_g(2)$	221.1	212			229	131.5	137.6	
E_{1g}	203.0	186	177.4	185.2	193	118.3	122	126.9
$E_{2g}(1)$	108.9	108	78.3	106.7	88	76.6	83	68.2
$E_{2g}(2)$	183.2		105.3	208.6	204	132.5	139.2	92.1
$E_{2g}(3)$	226.5	219		215.5	215	145.4	146	
Infrared								
A_u (TO)	180.5			165		130.8		
A_u (LO)	270.5					190.7		
E_{1u} (TO1)	176.6		135.4	138		120.3		115.1
E_{1u} (LO1)	186.9					122.2		
E_{1u} (TO2)	205.6		164.4	210		139.8		126.1
E_{1u} (LO2)	267.4					184.2		
Silent								
B_g (1)	88.8		49.6		90	74.6		39.0
B_g (2)	230.1		117.6		250	151.9		97.1
B_u (1)	124.4		196.8		123	79.0		139.5
B_u (2)	269.4		248.2		263	161.6		166.9
E_{2u}	169.8		158.0		193	109.4		110.5

the Raman spectra in Ref. 12 also show good consistency with our calculation. The Raman spectrum of LaBr$_3$ reported by Asawa gave six Raman-active lines.[11] Compared with the experimental values, the present calculation results give the maximal deviation of 6.7 cm^{-1}, a rms of absolute deviations of 5.1 cm^{-1}, and a rms of relative deviations of 4.7%. Therefore, the quantitative agreement seems excellent. To the best of our knowledge, the infrared spectra of LaBr$_3$ is not available in the literatures, while the infrared active modes of LaCl$_3$ for transverse optic modes can be found:[12] 138 cm^{-1} for the A_u mode and 165 and 210 cm^{-1} for two E_{1u} modes. Only one of the E_{1u} modes shows somewhat large deviation from the calculated value. As shown in Table III, the phonon frequencies and their symmetry assignments were also obtained from an analysis of the vibrational spectra of Pr^{3+} in LaCl$_3$ and LaBr$_3$,[14] including Raman-active, infrared-active, and silent modes. Some of them are in good agreement with our calculated values, while others exhibit rather large deviations, especially for the silent modes. Such large deviations are very likely due to the wrong experimental values because the vibronic spectra using Pr^{3+} ion as probe can lead to a large experimental error and even wrong assignment when the absorption peaks are very week or somewhat overlapped. In addition, our calculations for the phonon frequencies of LaCl$_3$ for the silent modes are consistent with those calculated using the central force method in Ref. 12. Assuming that the difference in structure of LaCl$_3$ and LaBr$_3$ is small and the force between atoms is approximately the same in LaCl$_3$ and LaBr$_3$, the change in phonon frequency for any given mode is dependent on the different mass of Cl and Br. As a result, the phonon frequencies of LaCl$_3$ are higher than those of LaBr$_3$.

In order to obtain the phonon dispersion curves throughout the Brillouin zone, the dynamical matrices are obtained $4 \times 4 \times 6$ grid of q points, and real-space force constants are then found by Fourier transform of the dynamical matrices. The dynamical matrix at an arbitrary wave vector q can then be calculated by an inverse Fourier transform. The acoustic sum rule is applied to force the three acoustic phonon frequencies at the Γ point equal to zero strictly as being implied by the translation symmetry. The calculated phonon dispersion curves along the high symmetry lines of the Brillouin zone and corresponding density of states of LaCl$_3$ and LaBr$_3$ are shown in Fig. 2. The experimental values for the neutron scattering data are not available in the literature. Both phonon structures are stable. For LaCl$_3$, it is found that there are three phonon bands with frequencies below about 115 cm^{-1}, frequencies between 125 and 245 cm^{-1}, and frequencies between 255 and 271 cm^{-1}. The frequency gaps are about 10 cm^{-1}. However, there is no frequency gap in the phonon density of states of LaBr$_3$. The highest phonon frequencies are 271 cm^{-1} for LaCl$_3$ and 191 cm^{-1} for LaBr$_3$.

D. Dielectric permittivity tensors

The macroscopic static dielectric permittivity tensor ε_0 is calculated by adding the ionic contribution to the electronic permittivity tensor ε_∞.[30] In other words, the static dielectric tensor can be decomposed in the contributions of different modes as follows:
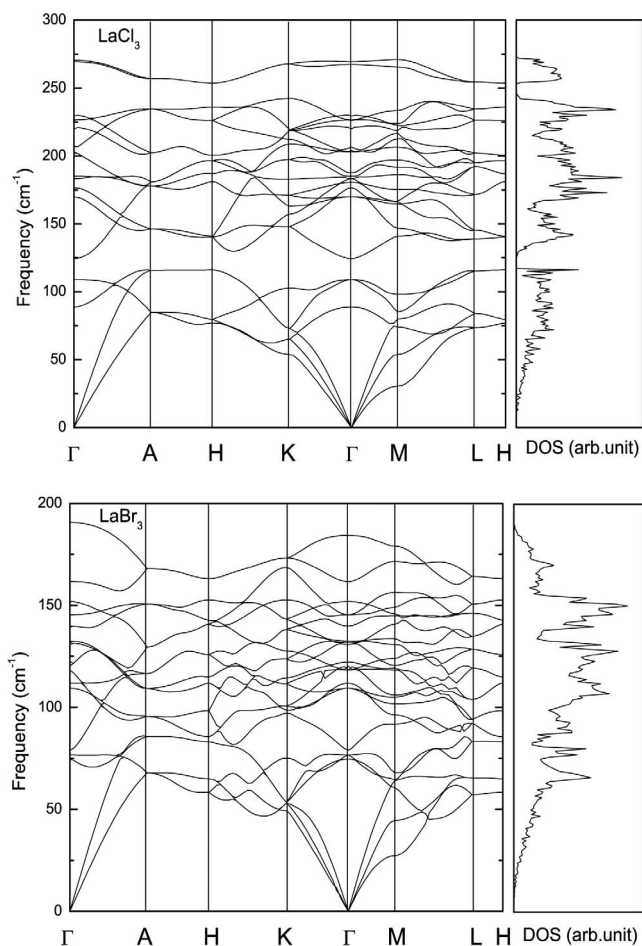

FIG. 2. Calculated phonon dispersion curves (left) and density of states (right) of LaCl$_3$ (top panel) and LaBr$_3$ (bottom panel).

$$\varepsilon_{\alpha\beta}^0(\omega) = \varepsilon_{\alpha\beta}^\infty + \sum_m \Delta\varepsilon_{m,\alpha\beta} = \varepsilon_{\alpha\beta}^\infty + \frac{4\pi}{\Omega_0} \sum_m \frac{S_{m,\alpha\beta}}{\omega_m^2}, \quad (2)$$

where Ω_0 is the volume of the primitive unit cell, ω_m is the frequency of vibration of normal mode m, and $S_{m,\alpha\beta}$ is the mode oscillator strength,[30] which can be determined by the eigendisplacements and the Born effective charge tensors. The electronic and static permittivity tensors of LaCl$_3$ and LaBr$_3$ have two independent components $\varepsilon^\parallel$ and $\varepsilon^\perp$, parallel and perpendicular to the c axis, respectively. The calculated values of $\varepsilon^\parallel$ and $\varepsilon^\perp$ are listed in Table IV. The average dielectric tensor of ε_∞ (or ε_0) can be expressed as $(2\varepsilon_\infty^\perp + \varepsilon_\infty^\parallel)/3$. The electronic dielectric tensors are near isotropic with a small anisotropy of 9.7 and 8.6 % for LaCl$_3$ and LaBr$_3$, respectively. The average electronic dielectric tensor of LaBr$_3$ (4.91) is larger than that of LaCl$_3$ (4.05) partly due to the larger polarizability of bromine.[37] The theoretical value for average electronic dielectric tensor of LaCl$_3$ is larger than the experimental one[15] by 9.2%, which is the usual error in the LDA to the density-functional theory.[38] Our calculated static dielectric tensor of LaCl$_3$ is comparable with the experimental value with an average deviation less than 5%. However, for LaBr$_3$, we are not able to find the experimental values in the literatures. The calculated average

TABLE IV. Electronic and static dielectric tensors of $LaCl_3$ and $LaBr_3$. The contributions of individual phonon modes to the static dielectric tensor are indicated. The phonon mode contributions to $\varepsilon^\perp$ (perpendicular to the c axis) come from the two infrared-active E_{1u} modes, while the contributions to $\varepsilon^\parallel$ (parallel to the c axis) come from the infrared-active A_u modes. $\Delta\varepsilon_m$ ($m=1,2,3$) are the contributions of the different phonon modes to the static dielectric tensor. The experimental dielectric tensors for $LaCl_3$ at temperature 82 K are also indicated between parentheses (Ref. 15).

	LaCl$_3$		LaBr$_3$	
	$\varepsilon^\perp$	$\varepsilon^\parallel$	$\varepsilon^\perp$	$\varepsilon^\parallel$
ε_∞	3.92 (3.71)	4.30 (3.71)	4.77	5.18
$\Delta\varepsilon_1$	1.71		0.53	
$\Delta\varepsilon_2$	1.79		3.25	
$\Delta\varepsilon_3$		5.34		5.84
ε_0	7.42 (8.02)	9.64 (9.56)	8.55	11.02

static dielectric tensor of $LaBr_3$ (9.37) is larger than that of $LaCl_3$ (8.16), which can be partly explained by the fact that the $LaBr_3$ has lower infrared-active phonon frequencies than that of $LaCl_3$. For the static dielectric tensor, the distinct anisotropy is 29.9 and 28.9 % for $LaCl_3$ and $LaBr_3$, respectively. Compared with the electronic dielectric tensors, the increasing anisotropy of the static dielectric tensors comes from the different contribution of the infrared-active modes A_u and E_{1u}. The contribution of the individual modes $\Delta\varepsilon_m$ to the static dielectric constant is also shown in Table IV. The two infrared-active A_u modes contribute to the static dielectric tensor parallel to the c axis, while the infrared-active mode E_{1u} contributes to the perpendicular component. For each infrared-active mode, the relevant components of the oscillator strength tensor S_m, the mode-effective charge vectors Z_m^*, the LO frequencies ω_m, and the LO-TO splitting $\Delta\omega$ are presented in Table V.

As can be seen in Table V, for both $LaCl_3$ and $LaBr_3$, the A_u mode has a much larger oscillator strength (S_m) and mode-effective charge (Z_m^*) than those of the $E_{1u}(1)$ and $E_{1u}(2)$ modes. However, the differences in phonon frequencies for modes A_u and E_{1u} are not too much. As a result, the A_u mode has the larger contribution to the static dielectric constant, compared with the E_{1u} modes. It is noticed that the largest LO-TO splitting is found in the A_u mode which involves the displacements of both the halogen and the lanthanum ions in z direction. However, the E_{1u} mode involves the

TABLE V. Oscillator strength tensor S_m (in 10^{-4} a.u.), mode-effective charge vectors Z_m^* (in units of $|e|$, where e is the electronic charge), LO frequencies ω_m (in cm^{-1}), and LO-TO splitting $\Delta\omega$ (in cm^{-1}) for each of the infrared-active modes of $LaCl_3$ and $LaBr_3$.

	LaCl$_3$				LaBr$_3$			
	S_m	Z_m^*	ω_m	$\Delta\omega$	S_m	Z_m^*	ω_m	$\Delta\omega$
A_u	3.86	6.07	270.5	90.0	2.58	7.16	190.7	59.2
E_{1u} (1)	1.18	3.16	186.9	10.3	0.20	1.84	122.2	1.9
E_{1u} (2)	1.67	3.44	267.4	61.8	1.63	5.51	184.2	44.4

displacements of both the halogen and the lanthanum ions in the x, y plane. The static dielectric tensors are more highly anisotropic than the electronic dielectric tensors due to the different contributions from the infrared-active modes A_u and E_{1u}.

Now we can estimate the light yield of $LaCl_3$:Ce and $LaBr_3$:Ce from the calculated dielectric constants. The overall quantum efficiency of the scintillation process is generally expressed as $\eta=\beta SQ$, where the β, S, and Q are the efficiencies of conversion, energy transfer, and luminescence, respectively.[39,40] The parameter β is approximately expressed as $\beta=1/(1+0.65\ K)$.[41] K, the energy loss parameter, is given by $K=0.244\times10^4(\varepsilon_\infty^{-1}-\varepsilon_0^{-1})(\hbar\omega_{LO})^{3/2}/(1.5E_g)$. Where ε_∞ and ε_0 are average electronic and static dielectric permittivity constants, respectively. ω_{LO} is the longitudinal optical phonon frequency. E_g, the band gap of the host, is 6.5 and 5.9 eV for $LaCl_3$ and $LaBr_3$, respectively, estimated from the excitation spectra.[42] The light yield L can be expressed as $L=[10^6/(2.3E_g)]\beta SQ$.[43] For an ideal situation, assuming that all electron-hole pair energy arrives at the luminescence center ($S=1$) and the quantum efficiency of luminescence center is to be unity ($Q=1$). The theoretically estimated light yield are 62 400 and 71 400 photons/MeV for $LaCl_3$:Ce and $LaBr_3$:Ce, respectively, on the basis of the calculated values of the dielectric constants and the highest longitudinal optical infrared phonon frequencies. Therefore, $LaCl_3$:Ce and $LaBr_3$:Ce are excellent scintillators with high light yield predicted by theoretical calculations, especially for LaBr:Ce. The experimental values mentioned in the introduction section reach 74 and 88 % of the theoretical values for $LaCl_3$:Ce and $LaBr_3$:Ce, respectively.

E. Thermodynamic properties

The thermodynamic functions of $LaCl_3$ and $LaBr_3$ can be determined by the entire phonon spectrum, assuming that the vibrational degrees of freedom of the lattice play a noticeable role while the electronic degrees of freedom are ignorable. In the present work, the phonon contribution to the Helmholtz free energy ΔF, the phonon contribution to the internal energy ΔE, the entropy S, and the constant-volume specific heat C_v, at temperature T are calculated using the formulas in Ref. 44 within the harmonic approximation,[45] shown in Fig. 3. ΔF and ΔE at zero-temperature represent the zero-point motion, which can be calculated from the expression as

$$\Delta F_0 = \Delta E_0 = 3nN\int_0^{\omega_{max}}\frac{\hbar\omega}{2}g(\omega)d\omega, \qquad (3)$$

where n is the number of atoms per unit cell, N is the number of unit cells, ω is the phonon frequencies, ω_{max} is the largest phonon frequency, and $g(\omega)$ is the normalized phonon density of states with $\int_0^{\omega_{max}}g(\omega)d\omega=1$. The calculated $\Delta F_0=\Delta E_0=12.1$ kJ/mol for $LaCl_3$ and 8.0 kJ/mol for $LaBr_3$. The zero-point motion contribution to the thermodynamic functions of $LaCl_3$ is more important than that of $LaBr_3$. The temperature-dependent ΔF and ΔE are higher for $LaCl_3$ than $LaBr_3$ since $LaCl_3$ has much higher average phonon frequencies and lower entropy. The calculated entropies of $LaCl_3$
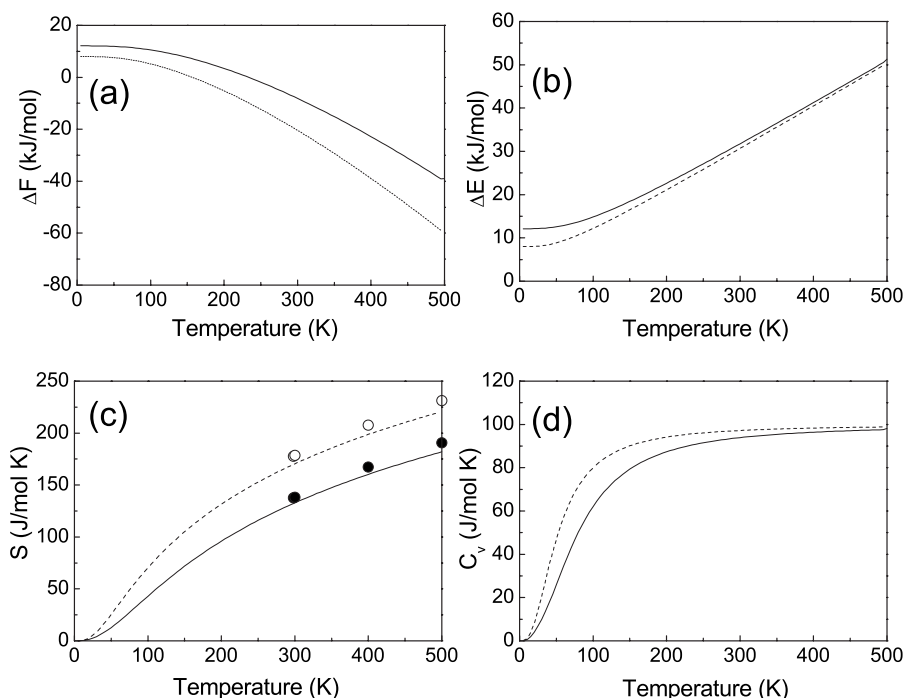
FIG. 3. The calculated phonon contribution to the Helmholtz free energy ΔF (a), the phonon contribution to the internal energy ΔE (b), the entropy S (c), and the constant-volume specific heat C_v (d) of LaCl$_3$ (solid lines) and LaBr$_3$ (dashed lines). The experimental values of entropy (solid circles for LaCl$_3$ and open circles for LaBr$_3$, Ref. [39]) are also shown in (c).

and LaBr$_3$ exhibit reasonable agreement with the experimental values[46] above room temperature. The experimental values are slightly larger by about 5% than the calculated values since the effects of anharmonicity are ignored and the theoretical lattice constants are used in the calculation. LaCl$_3$ is found to have lower entropy than LaBr$_3$, which can be explained by the smaller phonon density of states for LaCl$_3$ for low-frequency modes.

The constant-volume specific heats C_v are calculated and shown in Fig. 3(d). In the low-temperature limit, the two specific heats exhibit the expected T^3 power-law behavior, and they both approach at high temperatures the classical asymptotic limit of $C_v = 3nNk_B = 99.8$ J/mol K. The experimental C_v cannot be found, but the experimental constant-pressure heats C_p are 98.25, 103.486, and 107.545 J/mol K for LaCl$_3$ and 99.654, 103.685, and 106.871 J/mol K for LaBr$_3$ at temperatures of 300, 400, and 500 K, respectively,[46] which is systemically larger than the C_v. Due to the thermal-expansion caused by anharmonicity effects C_p is different than C_v. The relation between C_p and C_v is determined by[47]

$$C_P - C_V = \alpha_V^2(T)B_0 VT, \qquad (4)$$

where α_V is the volume thermal expansion coefficient, B_0 is the bulk modulus, V is the volume and T is absolute temperature. In order to deduce the theoretical C_p, the determination of thermal expansion coefficients is necessary, which is in progress.

IV. SUMMARY

The lattice dynamics and thermodynamic properties of LaCl$_3$ and LaBr$_3$ using density-functional perturbation theory and pseudopotential methods are performed. For both LaCl$_3$ and LaBr$_3$, the relaxed lattice constants are found to be in good agreement with experimental ones with the errors less than 2.2%.

The anisotropy in the Born effective charge tensors is observed. For La and halogen ions in some directions, these effective charges are found to be larger than the nominal ionic charge, indicating a mixed covalent-ionic bonding between La and halogen ions. The electronic and static permittivity tensors of LaCl$_3$ and LaBr$_3$ have two independent components $\varepsilon^{\parallel}$ and $\varepsilon^{\perp}$, parallel and perpendicular to the c axis, respectively. A detailed analysis of the contribution of the different vibration modes to the static dielectric constant has been performed. The mode-effective charges and the oscillator strengths are also calculated. The static dielectric tensors show to be much more anisotropic than the electronic dielectric tensors due to the different infrared-active modes A_u and E_{1u}.

The phonon frequencies at the Γ point of the Brillouin zone are calculated and their symmetry assignments are given. The calculated Raman-active phonon frequencies are in excellent agreement with the experimental values. The difference in phonon frequencies between LaCl$_3$ and LaBr$_3$ can be analyzed by the different mass of Cl and Br. The phonon dispersion curves along the high symmetry lines of the Brillouin zone and the corresponding density of states for LaCl$_3$ and LaBr$_3$ are computed. The highest phonon frequencies are 271 cm^{-1} for LaCl$_3$ and 191 cm^{-1} for LaBr$_3$. The density of states of LaCl$_3$ shows three phonon bands while LaBr$_3$ has a continuous density structure. Based on the calculated values of the dielectric constants and the highest longitudinal optical infrared phonon energy, the theoretically estimated light yield are as high as 62 400 and 71 400 photons/MeV for LaCl$_3$:Ce and LaBr$_3$:Ce, respectively.

The thermodynamics properties including the phonon contribution to the Helmholtz free energy ΔF, the phonon contribution to the internal energy ΔE, the entropy S, and the constant-volume specific heat C_v are present within the harmonic approximation. Their difference for $LaCl_3$ and $LaBr_3$ can be understood in terms of the phonon density of states.

---

*lbo@mail.tongji.edu.cn

[1] P. Dorenbos, C. W. E. van Eijk, H. U. Gudel, K. W. Kraemer, and E. V. D. van Loef, International Patent WO/016944 A2, 16 February 2000.

[2] P. Dorenbos, C. W. E. van Eijk, H. U. Gudel, K. W. Kraemer, and E. V. D. van Loef, International Patent WO/016945 A2, 16 February 2001.

[3] A. Iltisa, M. R. Mayhughb, P. Mengeb, C. M. Rozsab, O. Sellesc, and V. Solovyev, Nucl. Instrum. Methods Phys. Res. A **563**, 359 (2006).

[4] E. V. D. van Loef, Nucl. Instrum. Methods Phys. Res. A **486**, 254 (2002).

[5] E. V. D. van Loef, P. Dorenbos, C. W. E. van Eijk, H. U. Gudel, and K. W. Kraemer, Appl. Phys. Lett. **79**, 1573 (2001).

[6] E. V. D. van Loef, P. Dorenbos, C. W. E. van Eijk, H. U. Gudel, and K. W. Kraemer, Appl. Phys. Lett. **77**, 1467 (2000).

[7] K. S. Shah, J. Glodo, M. Klugerman, W. W. Moses, and M. J. Weber, IEEE Trans. Nucl. Sci. **NS-50**, 2410 (2003).

[8] L. A. Riseberg and H. W. Moss, Phys. Rev. Lett. **19**, 1423 (1967).

[9] L. A. Riseberg and H. W. Moss, Phys. Rev. **174**, 429 (1968).

[10] C. K. Asawa, R. A. Satten, and O. M. Stafsudd, Phys. Rev. **168**, 957 (1968).

[11] C. K. Asawa, Phys. Rev. **173**, 869 (1968).

[12] J. Murphy, H. H. Caspers, and R. A. Buchanan, J. Chem. Phys. **40**, 743 (1964).

[13] E. Cohen and H. W. Moos, Phys. Rev. **161**, 268 (1967).

[14] I. Richman, S. Robert, and W. Eugene, J. Chem. Phys. **39**, 1833 (1963).

[15] D. W. Berreman and F. C. Unterwald, Phys. Rev. **174**, 791 (1968).

[16] X. Gonze, J. M. Beuken, R. Caracas, F. Detraux, M. Fuchs, G. M. Rignanese, L. Sindic, M. Verstraete, G. Zerah, F. Jollet, M. Torrent, A. Roy, M. Mikami, P. Ghosez, J. Y. Raty, and D. C. Allan, Comput. Mater. Sci. **25**, 478 (2002).

[17] The ABINIT code is a common project of the Université Catholique de Louvain, and other contributors (URL http://www.abinit.org)

[18] S. Goedecker, SIAM J. Sci. Comput. (USA) **18**, 1605 (1997).

[19] M. C. Payne, M. P. Teter, D. C. Allan, T. A. Arias, and J. D. Joannopoulos, Rev. Mod. Phys. **64**, 1045 (1992).

[20] X. Gonze, Phys. Rev. B **54**, 4383 (1996).

[21] J. P. Perdew and Y. Wang, Phys. Rev. B **45**, 13244 (1992).

[22] D. M. Ceperley and B. J. Alder, Phys. Rev. Lett. **45**, 566 (1980).

[23] C. Hartwigsen, S. Goedecker, and J. Hutter, Phys. Rev. B **58**, 3641 (1998).

[24] N. Troullier and J. L. Martins, Phys. Rev. B **43**, 1993 (1991).

[25] M. Fuchs and M. Scheffler, Comput. Phys. Commun. **119**, 67 (1999).

[26] W. H. Press, B. P. Flannery, S. A. Teukolsky, and W. T. Vetterling, *Numerical Recipes, The Art of Scientific Computing (FORTRAN Version)* (Cambridge University Press, Cambridge, 1989).

[27] H. B. Schlegel, J. Comput. Chem. **3**, 214 (1982).

[28] X. Gonze, Phys. Rev. B **55**, 10337 (1997).

[29] X. Gonze, D. C. Allan, and M. P. Teter, Phys. Rev. Lett. **68**, 3603 (1992).

[30] X. Gonze and C. Lee, Phys. Rev. B **55**, 10355 (1997).

[31] H. J. Monkhorst and J. D. Pack, Phys. Rev. B **13**, 5188 (1976).

[32] N. H. Kiess and G. H. Dieke, J. Chem. Phys. **45**, 2729 (1966).

[33] W. H. Zachariasen, J. Chem. Phys. **16**, 254 (1948).

[34] P. Ghosez, J.-P. Michenaud, and X. Gonze, Phys. Rev. B **58**, 6224 (1998).

[35] M. Mikami and S. Nakamura, J. Alloys Compd. **408-412**, 687 (2006).

[36] R. Vali, Comput. Mater. Sci. **37**, 300 (2006).

[37] D. Bunimovich and A. Katzir, Appl. Opt. **32**, 2045 (1993).

[38] G. M. Rignanese, X. Gonze, G. Jun, K. Cho, and A. Pasquarello, Phys. Rev. B **69**, 184301 (2004).

[39] G. Blasse, Comput. Mater. Sci. **6**, 1465 (1994).

[40] M. Mikami, S. Nakamura, M. Itoh, K. Nakajima, and T. Shishido, J. Lumin. **102-103**, 7 (2003).

[41] D. J. Robbins, J. Electrochem. Soc. **127**, 2694 (1980).

[42] P. Dorenbos, E. V. D. van Loef, A. P. Vink, E. van der Kolk, C. W. E. van Eijk, K. W. Krer, H. U. Gel, W. M. Higgins, and K. S. Shah, J. Lumin. **117**, 147 (2006).

[43] A. Lempicki and A. J. Wojtowicz, J. Lumin. **60-61**, 942 (1994).

[44] C. Lee and X. Gonze, Phys. Rev. B **51**, 8610 (1995).

[45] A. A. Maradudin, E. W. Montroll, G. H. Weiss, and I. P. Ipatova, *Theory of Lattice Dynamics in the Harmonic Approximation*, 2nd ed. (Academic, New York, 1971).

[46] I. Barin, *Thermochemical Data of Pure Substances*, 3rd ed. (VCH, Weinheim, 1995).

[47] H. B. Callen, *Thermodynamics and an Introduction to Thermostatistics* (Wiley, New York, 1985).